Bulk and surface critical behavior of the three-dimensional Ising model and conformal invariance

Youjin Deng[1] and Henk W. J. Blöte[1,2]
[1]*Faculty of Applied Sciences, Delft University of Technology, P.O. Box 5046, 2600 GA Delft, The Netherlands*
[2]*Lorentz Institute, Leiden University, P.O. Box 9506, 2300 RA Leiden, The Netherlands*
(Received 28 February 2003; published 27 June 2003)

Using a continuous cluster Monte Carlo algorithm, we investigate the critical three-dimensional Ising model in its anisotropic limit. From the ratio of the magnetic correlations in the strong- and the weak-coupling directions, we determine the length ratio relating the isotropic Ising model and the anisotropic limit. On this basis, we simulate the critical Ising model on a spherocylinder $S^2\times\mathbb{R}^1$, i.e., a curved geometry obtained from a conformal mapping of the infinite space $\mathbb{R}^3$. From correlation lengths along the spherocylinder, combined with the prediction of conformal invariance, we estimate the magnetic and thermal scaling dimensions as $X_h=0.5182(6)$ and $X_t=1.419(7)$, respectively. The behavior of the Binder cumulant is also determined in the limit of an infinitely long spherocylinder. Next, free boundary conditions are imposed on the equators of the spherocylinder, and thus the geometry $S^1\times S^+\times\mathbb{R}^1$ is obtained. The surface magnetic scaling dimension is estimated as $X_h^{(s)}=1.263(5)$. The consistency of the aforementioned estimations and existing results confirms that the three-dimensional Ising model is conformally invariant. Further, the precision of these results reveals that, as in two dimensions, conformal mappings provide a powerful tool to investigate critical phenomena. With the continuous cluster algorithm, we also perform simulations of systems inside a conventional solid cylinder. The surface magnetic correlation length differs, within the estimated error margin, by a factor $\pi/2$ from that along a half spherocylinder $S^1\times S^+\times\mathbb{R}^1$ with the same radius.

DOI: 10.1103/PhysRevE.67.066116 PACS number(s): 05.50.+q, 64.60.Cn, 64.60.Fr, 75.10.Hk

I. INTRODUCTION

Applications of conformal invariance in two dimensions have been explored extensively and produced fruitful results both for bulk and for surface critical phenomena [1–4]. Conformal mappings provide relations between critical systems in different geometries. A well-known and particularly useful example is Cardy's mapping between an infinite plane and the surface of an infinitely long cylinder, which transforms the algebraic decay of correlations in the plane into an exponential decay along the cylinder [5,6]. Because a cylinder is pseudo-one-dimensional, its numerical investigation is simpler than that of a two-dimensional plane. This mapping can be generalized to any number of dimensions [6]. In three dimensions, Cardy's mapping transforms an infinite space $\mathbb{R}^3$ into a pseudo-one-dimensional geometry $S^2\times\mathbb{R}^1$, i.e., a curved geometry extending the surface of a sphere S^2 into another dimension $\mathbb{R}^1$. Thus, one also expects that, as in two dimensions, Cardy's mapping also provides a significant help in numerical studies of critical phenomena. In particular, we need such studies because exact results are scarce in three dimensions. However, the nonzero net curvature of the geometry $S^2\times\mathbb{R}^1$ poses a serious obstacle for numerical investigations.

Recently, we solved this problem for the case of the Ising model by using the Hamiltonian limit of the lattice Ising model and a continuous cluster Monte Carlo algorithm [7,8]. The key ingredient of this infinitely anisotropic model is that one of its dimensions is continuous, so that the problem of discretization for one of the lattice directions is avoided. In two dimensions, we have numerically studied a conformal mapping between an infinite plane and a spheroid [9]. Special cases of the spheroid include the surfaces of an infinitely long cylinder, of a sphere, and of a flat disc. Thus, this mapping includes Cardy's transformation as a special case. A brief report has also been published about the confirmation of Cardy's mapping in three dimensions [7], in which the aforementioned geometry $S^2\times\mathbb{R}^1$ was named a ''spherocylinder.'' In the present paper, the techniques involved in Ref. [7] will be described in more detail. Moreover, by mapping the semiinfinite space $\mathbb{R}^2\times\mathbb{R}^+$ onto the half spherocylinders $S^2\times\mathbb{R}^+$ and $S^1\times S^+\times\mathbb{R}^1$, respectively, we investigate the surface criticality of the Ising model in three dimensions.

The present work also includes simulations of the Ising model inside a conventional solid cylinder. Compared to the aforementioned half spherocylinder, the conventional solid cylinder has a zero net curvature. However, numerical simulations suffer from complications due to its curved surface. Such a difficulty is avoided by using the Hamiltonian limit of the lattice Ising model and the continuous cluster algorithm. Free boundary conditions are imposed on the surface of the conventional solid cylinder, and correlation functions along the cylinder are sampled. In fact, the conventional solid cylinder is closely related to the half spherocylinder $S^1\times S^+\times\mathbb{R}^1$. The former object is obtained by replacing the half sphere of the latter object by the interior of a circle.

The outline of this paper is as follows. In Sec. II, we briefly describe the conformal mapping between the infinite space $\mathbb{R}^3$ and the spherocylinder $S^2\times\mathbb{R}^1$, and those between the semiinfinite space $\mathbb{R}^2\times\mathbb{R}^+$ and the half spherocylinders $S^2\times\mathbb{R}^+$ and $S^1\times S^+\times\mathbb{R}^1$. From the prediction of conformal invariance, the expressions of the bulk and surface correlation functions are derived for the spherocylinder and both half spherocylinders, respectively. Section III recalls the Hamiltonian limit of the lattice Ising model, and the continuous cluster algorithm. During the Monte Carlo simulations, the magnetic correlations over half linear system sizes were sampled both in the strong- and in the weak-coupling direc-

tions. By demanding asymptotic symmetry of these correlation functions, we obtain the anisotropic rescaling factor relating the isotropic version of the Ising model and its anisotropic limit. On this basis, asymptotically isotropic Ising models are defined on the spherocylinder and inside the conventional solid cylinder. In Sec. IV, numerical results are presented for the spherocylinder, the half spherocylinders, and the solid cylinder, respectively. A short discussion is given in Sec. V.

II. CONFORMAL MAPPING

In two dimensions, one may parametrize the infinite plane as a complex number $z=x+iy$. Cardy's transformation is then expressed as $z'=R\ln z$ [5]. The geometry of z' can be interpreted as the surface of an infinitely long cylinder or a flat strip with periodic boundary conditions. For a critical system with a scaling dimension X, Cardy's mapping yields the correlation length along the cylinder as

$$\xi_R = R/X, \tag{1}$$

where R is the radius of the cylinder [4].

This mapping can be generalized to any number of dimensions [6]. In three dimensions, one may express the flat space $\mathbb{R}^3$ in spherical coordinates (r,φ). Cardy's mapping is then described by the coordinate transformation:

$$(r,\theta,\varphi)=(e^{u/R},\theta,\varphi) \quad (-\infty<u<\infty), \tag{2}$$

where R is a free parameter. Thus, a geometry expressed by the variables (u,θ,φ) in Eq. (2) is reached. It is obvious that this geometry is analogous to the surface of an infinite cylinder as mentioned earlier. The latter object can be recognized as the extension of a circle S^1 into another dimension $\mathbb{R}$. Analogously, the former geometry can be obtained by extending a sphere S^2 into another dimension $\mathbb{R}$. This dimension is perpendicular to the surface of the sphere, which, unfortunately, cannot be visualized in three-dimensional space. Taking into account this analogy, we named in Ref. [7] the three-dimensional geometry $S^2\times\mathbb{R}$ a spherocylinder.

The reason why Eq. (2) is conformal is as follows. First, the metric of the flat space $\mathbb{R}^3$ is expressed, in spherical coordinates, by the invariant line element

$$ds^2=dr^2+r^2(d\theta^2+\sin^2\theta d\varphi^2) \quad (0\leqslant\theta\leqslant\pi, 0\leqslant\varphi<2\pi). \tag{3}$$

Under the transformation (2), Eq. (3) becomes [6]

$$ds^2=R^{-2}e^{2u/R}[du^2+R^2(d\theta^2+\sin^2\theta d\varphi^2)], \tag{4}$$

where $ds'^2=du^2+R^2(d\theta^2+\sin^2\theta d\varphi^2)$ reflects the natural metric of the spherocylinder $S^2\times\mathbb{R}^1$. Equation (4) shows that the line elements ds^2 and ds'^2 differ only by a position-dependent factor $R^{-2}e^{2u/R}$. Thus, the mapping (2) is conformal.

Under a conformal mapping $(\vec{r}\to\vec{r}')$, a multipoint correlation function covariantly transforms as [4]

$$\langle\sigma_1(\vec{r}_1)\sigma_2(\vec{r}_2)\cdots\rangle_{\vec{r}}=b(\vec{r}_1)^{-X_1}b(\vec{r}_2)^{-X_2}\cdots \times\langle\sigma_1(\vec{r}_1')\sigma_2(\vec{r}_2')\cdots\rangle_{\vec{r}'}, \tag{5}$$

where σ_i is a scaling operator (e.g., associated with the magnetization density or the energy density) and $b(\vec{r})$ is the rescaling factor, which reads as $b(\vec{r})^2=ds^2/ds'^2$.

In the infinite space $\mathbb{R}^3$, the critical two-point correlation function behaves as

$$\langle\sigma(\vec{r}_1)\sigma(\vec{r}_2)\rangle_{\mathbb{R}^3}\propto|\vec{r}_2-\vec{r}_1|^{-2X}. \tag{6}$$

Equations (2), (5), and (6) yield the correlation function along the spherocylinder as

$$\langle\sigma(u_1,\theta,\varphi)\sigma(u_2,\theta,\varphi)\rangle_{S^2\times\mathbb{R}^1} \propto R^{-2X}(e^{|u_1-u_2|/2R}-e^{-|u_1-u_2|/2R})^{-2X}. \tag{7}$$

For $|u_1-u_2|\gg 0$, Eq. (7) reduces to

$$\langle\sigma(u_1,\theta,\varphi)\sigma(u_2,\theta,\varphi)\rangle\propto R^{-2X}e^{-X|u_1-u_2|/R}, \tag{8}$$

so that the relationship (1) follows again.

However, applications of Eq. (1) in three dimensions are rather scarce so far. The reason is that the spherocylinder $S^2\times\mathbb{R}^1$ has a nonzero net curvature. For numerical investigations, a curved geometry does not readily accommodate a sequence of regular lattices. For the special case of the spherical model, Eq. (8) has been verified analytically by Cardy [6]. Janke and Weigel approximated the S^2 sphere by the surface of a cube [10]. Their results for the Ising model with finite size R satisfy Eq. (8) up to a proportionality constant, which has to be determined empirically.

Under the mapping (2), the half infinite space $\mathbb{R}^2\times\mathbb{R}^+$ conformally transforms into the half spherocylinder $S^1\times S^+\times\mathbb{R}$, i.e., a geometry also described by the natural metric ds'^2 in Eq. (4), but with $0\leqslant\theta\leqslant\pi/2$. Thus, this geometric object has a surface at the equators ($\theta=\pi/2$) of the spheres. The pair correlation on the surface of the half space $\mathbb{R}^2\times\mathbb{R}^+$ follows from the formula (6), except that the bulk scaling dimension X is replaced by the surface dimension $X^{(s)}$ [4]. Thus, the surface correlation at the equators of the half spherocylinder is also described by Eq. (7), but with a substitution of X by $X^{(s)}$.

Next, we consider another conformal mapping between the semi-infinite space $\mathbb{R}^2\times\mathbb{R}^+$ and a half spherocylinder $S^2\times\mathbb{R}^+$, also described by the metric ds'^2 in Eq. (4), but with $u\geqslant 0$. This mapping is different from Eq. (2) and is conveniently described in two steps. First, the formula [11]

$$\vec{r}'/r'^2=\vec{r}/r^2+\hat{I}/2, \tag{9}$$

maps spheres onto spheres in three dimensions, and the space $\mathbb{R}^3$ is transformed into itself [11]. Here, $\hat{I}$ is an arbitrary fixed unit vector. Under the mapping (9), the plane $\hat{I}\cdot\vec{r}=0$, which corresponds to a spherical surface of an infinite radius, is conformally mapped onto the surface of a unit sphere with the center at $\hat{I}$. Meanwhile, the half spaces $\hat{I}\cdot\vec{r}$

>0 and $\hat{I}\cdot\vec{r}<0$ are transformed, respectively, into the interior and exterior of this unit sphere. The homogeneous translation

$$\vec{r}''=\vec{r}-\hat{I} \tag{10}$$

shifts the center of the sphere to the origin of the double-primed coordinate system.

The profile of a scaling operator σ in the semi-infinite space $\mathbb{R}^2\times\mathbb{R}^+$ behaves as [4]

$$\langle\sigma(\vec{r})\rangle_{\mathbb{R}^2\times\mathbb{R}^+}\propto y^{-X}, \tag{11}$$

where $y\gg 0$ is the distance of a point $\vec{r}$ to the surface. Equations (9) and (10) yield the rescaling factor $b(\vec{r})$ of the conformal mapping $(\vec{r}\to\vec{r}'')$ as [11]

$$b(\vec{r})=1+\hat{I}\cdot\vec{r}+r^2/4=4/(\vec{r}''-\hat{I})^2. \tag{12}$$

From Eqs. (5) and (9)–(12), the quantity $\langle\sigma(\vec{r}'')\rangle$ inside a unit sphere follows from [4,11]

$$\langle\sigma(\vec{r}'')\rangle\propto|1-(r'')^2|^X, \tag{13}$$

where $r''\leqslant 1$ is the distance of the point $\vec{r}''$ to the center of sphere.

Next, we apply Eq. (2) to conformally map this unit sphere onto the half spherocylinder $S^2\times\mathbb{R}^+$. The profile (13) is then covariantly transformed into

$$\langle\sigma(u,\theta,\varphi)\rangle_{S^2\times\mathbb{R}^+}\propto R^{-X}(e^{|u_1-u_2|/2R}-e^{-|u_1-u_2|/2R})^{-2X}, \tag{14}$$

which differs from Eq. (7) by a factor R^{-X}.

Moreover, Eqs. (9), (10), and (2) transform the quarter-infinite space $\mathbb{R}^1\times\mathbb{R}^+\times\mathbb{R}^+$ into a quarter of the infinite spherocylinder $S^1\times S^+\times\mathbb{R}^+$, described by ds'^2 in Eq. (4) but with $0\leqslant\theta\leqslant\pi/2$ and $u\geqslant 0$. Therefore, the profile of the surface scaling operator at the equators should follow from Eq. (14) except that the exponent X is replaced by the surface scaling dimension $X^{(s)}$.

III. MODEL AND ALGORITHM

In this section, we briefly recall the Hamiltonian limit of the Ising model and the continuous cluster algorithm [8]. The applications to the spherocylinder and the conventional solid cylinder are also described.

The three-dimensional Ising model with anisotropic couplings is described by the Hamiltonian

$$\mathcal{H}/k_BT=-\sum_{x,y,z}[K_{xy}s_{x,y,z}(s_{x+1,y,z}+s_{x,y+1,z}) + K_z s_{x,y,z}s_{x,y,z+1}], \tag{15}$$

where the integers $1\leqslant x,y\leqslant L$ and $1\leqslant z\leqslant L'$ label the sites of a cubic lattice, K_{xy} and K_z are the coupling strengths along bonds perpendicular and parallel to the z direction, respectively. The spins can assume the values $s_{x,y,z}=\pm 1$.

In the limit that the interactions in the z direction are infinitely strong, the couplings K_{xy} and K_z become

$$K_{xy}=\epsilon/t,\quad \exp[-2K_z]=\epsilon,\quad (\epsilon\to 0), \tag{16}$$

where t parametrizes the temperature and ϵ is an infinitely small number. The anisotropic model defined by Eqs. (15) and (16) is equivalent to the quantum transverse Ising model on the square lattice [12,13]:

$$\mathcal{H}_{\rm qm}=-\sum_{x,y}[s^z_{x,y}(s^z_{x+1,y}+s^z_{x,y+1})+ts^x_{x,y}], \tag{17}$$

where $s^z_{x,y}$ and $s^x_{x,y}$ are Pauli matrices, and t represents a transverse field in the x direction.

For such an infinitely anisotropic system, the physical size in the z direction diverges as $1/\epsilon$, because the correlation length in this direction is of the order of $1/\epsilon$ [12,13]. In order to keep the correlation length finite, one may rescale as $z'=z\epsilon$ so that the z' dimension becomes continuous. This means that there is an infinite number of spins per physical length unit. As a result, the simple-cubic lattice reduces to L^2 lines originating from the sites of a $L\times L$ square lattice. The spins on these lines form ranges of $+/-$ signs, and the total number of interfaces between these ranges is of the order of L^3.

Monte Carlo simulations of this continuous system are realized by the application of a continuous cluster algorithm. This algorithm uses the positions of the aforementioned interfaces as the dynamical variables. The full description has been given in Ref. [8]. Here, we summarize the essential points. We start from a discrete Ising model and use bond variables as defined in the random cluster model [14]. During the formation of a cluster, the bond between nearest-neighbor spins of the same sign is ''frozen'' with a probability $P=1-\exp(-2K)$ or ''broken'' with the probability $1-P$. A cluster is then formed by spins connected to one another by these frozen bonds. The formation and flipping of these clusters lead to highly efficient Monte Carlo methods, which suppress the critical slowing down that is prominent in the Metropolis algorithm. In the Swendsen-Wang cluster method [15], the whole lattice is decomposed into a sequence of clusters. In the Wolff version of the cluster algorithm [16], only one cluster is formed and flipped during a Monte Carlo step. For the anisotropic Ising model defined by Eqs. (15) and (16), the probability P in the xy plane and z direction is of the order of ϵ and $1-\epsilon$, respectively. Thus, the strong-coupling bonds connect many spins in the z direction until a break occurs with a probability of the order of ϵ per bond. Spins between these breaks in the z direction form clusters of $+/-$ signs of with lengths of the order of $1/\epsilon$. After the rescaling described above, these z direction clusters reduce to ranges of $+/-$ signs, of which the length is now of the order of 1. Moreover, the average distance of the frozen weak-coupling bonds along the z direction is also of the order of 1. These weak-coupling bonds serve as ''bridges'' between neighboring lines to connect ranges of the same sign, and help to build clusters in the xy plane. As a result, continuous Wolff-like and Swendsen-Wang-like cluster algo-

rithms can be formulated for this anisotropic limit. The application of a continuous Wolff-like algorithm, combined with finite-size-scaling analysis, yields [8] the critical point as $t_c = 3.04438(2)$ for the model defined by Eqs. (15) and (16). The precision is good in comparison with existing results [17,18], and reflects the efficiency of the aforementioned continuous cluster algorithm.

Since our purpose is the application of conformal mappings, we have to restore isotropy asymptotically. This can be done by choosing an appropriate aspect ratio $\alpha = L_z'/L_{xy}$, where L_z' and $L_{xy} = L$ are linear system sizes in the z' direction and the xy plane, respectively. In Ref. [8], we determined the critical Binder cumulant as a function of the length ratio α. Matching this universal function with the case of the isotropic Ising model [19–21], we showed that the asymptotic isotropy of this Hamiltonian limit is restored for $\alpha_0 = 0.886(7)$. Here, we proceed differently. We sampled the critical magnetic correlations over half linear system sizes in the strong- and weak-coupling directions, respectively, of which the amplitude ratio d_m is defined as

$$d_m(\alpha, L) = \frac{\sum_{x,y} \int dz' \langle 2\sigma(x,y,z')\sigma(x,y,z'+\alpha L/2)\rangle}{\sum_{x,y} \int dz' \langle \sigma(x,y,z')[\sigma(x+L/2,y,z') + \sigma(x,y+L/2,z')]\rangle}. \tag{18}$$

This amplitude ratio d_m is a function of the length ratio α and the linear size L. The aforementioned isotropy means that the magnetic correlations in the z direction are equal to those in the x and y directions, and thus $d_m(\alpha_0, L) = 1$. Taking into account finite-size effects, we Taylor expand $d_m(\alpha, L)$, using logarithmic scales for d_m and α, as

$$\ln d_m(\alpha, L) = a_1(\ln\alpha - \ln\alpha_0) + a_2(\ln\alpha - \ln\alpha_0)^2 + bL^{y_a} + cL^{y_a}(\ln\alpha - \ln\alpha_0) + \cdots, \tag{19}$$

where a_1, a_2, b, and c are unknown parameters, and the correction with the exponent y_a is due to the microscopic deviations from isotropy of the Hamiltonian limit of the Ising model. In two dimensions, such a correction has been investigated in detail [9]. It was found that $y_a \approx -2 = y_i$, where y_i is the exponent of the irrelevant field for the two-dimensional Ising model. Here, we assume that this relation also holds in three dimensions so that $y_a = y_i = -0.821(5)$, where the value of y_i was taken from Refs. [9,19–21]. On the basis of the least-squares criterion, Eq. (19) was fitted to the Monte Carlo data. We find that $a_1 = 0.505(2)$, $a_2 = 0.06(1)$, $b = 0.375(7)$, $c = 2.8(3)$, and $\alpha_0 = 0.8881(2)$, which provides a significant improvement over our previous result $\alpha_0 = 0.886(7)$ [8].

As a result, the new coordinate $z'' = z'/\alpha_0$ restores the isotropy asymptotically for systems consisting of L^2 lines with physical length L in the large-L limit. Due to periodic boundary conditions, each of these lines can be recognized as a circle S^1. This enables one [7,9] to represent the ''lattice structure'' on a sphere S^2 by L evenly spaced circles with a varying radius, such that the strong couplings are along the φ direction while the weak couplings are between the adjacent circles. The location of the kth circle is $\theta_k = (k - \frac{1}{2})\pi/L$ ($k = 1,2,\ldots,L$), and the corresponding circumference is $2L\sin\theta_k$, which accounts for the S^2 curvature. Since the probability of a weak-coupling bond is defined *per unit of length*, and the adjacent circles on a sphere have different radii, the distribution of these weak-coupling bonds still requires a length scale. It was chosen as the average length scale of both circles. Therefore, the circumference of the sphere is $2L$, and the radius is L/π [7,9]. The validity of this method, i.e., asymptotic spherical symmetry of such systems, has been confirmed in Ref. [9]. Extension of this lattice structure of a sphere into another dimension yields the approximation of the spherocylinder $S^2 \times \mathbb{R}^1$ [7].

The critical point for systems on the spherocylinder is identical to that in the flat space $\mathbb{R}^3$. Arguments are (a) the lattice structures in these two geometries are same on a microscopic scale and (b) for finite systems L, the discretization in θ leads to an integrated effect on the average coupling strength, which is proportional to L^{-2} according to the trapezium rule. Under renormalization, this effect leads to corrections proportional to L^{y_t-2}. Since the thermal scaling exponent $y_t < 2$ for the two- and three-dimensional Ising models, this effect will vanish for $L \to \infty$. In two dimensions, we have studied the Ising model on a sphere [7,9], and confirmed that the leading corrections for finite systems are of the order of L^{y_t-2}.

Analogous procedures can be applied to the interior of a circle, i.e., a disc geometry. In this case, the lattice structure on the disc is also represented by L evenly distributed circles, but the kth circle is simply located at $r_k = (k - \frac{1}{2})$. Thus, the radius of the disc is just that of the largest circle $\pi(2L - 1)$. The conventional solid cylinder is obtained by extending this disc geometry into another dimension with a discrete lattice structure.

IV. NUMERICAL RESULTS

By applying the aforementioned continuous Wolff-like cluster algorithm, we have simulated the Hamiltonian limit of the Ising model in the following geometries.

A. Spherocylinder with periodic boundary conditions

For systems on a spherocylinder, the values of L were taken as 4,6,8,10,12,14,16,20. The finite size in the $\mathbb{R}$ direc-

tion was taken as $nL=8L$. Periodic boundary conditions were imposed in the u direction ($u=0$ and $u=8L$). Later, we will show that $n=8$ is large enough to approximate the geometry $S^2\times\mathbb{R}^1$. We sampled the magnetic correlation function $g_m(r)$ in the u direction, which is defined by [7]

$$g_m(r)=\frac{1}{V}\sum_{u,\theta}\int_0^{2\pi}d\varphi\frac{L}{\pi}\sin\theta\langle\sigma(u,\theta,\varphi)\sigma(u+r,\theta,\varphi)\rangle. \tag{20}$$

Since couplings are different in the φ direction and in the other two directions, there are two ways to represent the energy density: the density of the interfaces and of the nearest-neighbor interactions in the weak-coupling directions. We chose the latter one

$$e_{nn}=\frac{1}{V}\sum_{u,\theta}\int_0^{2\pi}d\varphi\frac{L}{\pi}\sin\theta\langle\sigma(u,\theta,\varphi)\sigma(u+1,\theta,\varphi)\rangle, \tag{21}$$

in order to sample the energylike correlation $g_e(r)$:

$$g_e(r)=\frac{1}{V}\sum_{u,\theta}\int_0^{2\pi}d\varphi\frac{L}{\pi}\sin\theta\langle\sigma(u,\theta,\varphi)\sigma(u+1,\theta,\varphi)\times\sigma(u+r,\theta,\varphi)\sigma(u+r+1,\theta,\varphi)\rangle-e_{nn}^2. \tag{22}$$

For finite systems, there is a correction $\propto L^{y_t-2}$ as mentioned earlier. Compared to the irrelevant scaling exponent $y_i=-0.821(5)$ in three dimensions [9,19–21], the correction with the power $y_c=y_t-2=-0.413$ is expected to dominate over that with y_i.

In the continuum limit, the behavior of the magnetic energylike correlations $g_m(r)$ and $g_e(r)$, respectively, follows from Eq. (7). Taking into account finite-size effects yields the correlation length ξ_L as

$$\xi_L^{-1}=\frac{X}{R}(1+aL^{y_c}+bL^{y_i})=\frac{\pi X}{L}(1+aL^{y_c}+bL^{y_i}). \tag{23}$$

Due to the periodicity in the u direction, correlations build up over two distances r and $nL-r$. Thus, the correlation function $g(r,L)$ for finite systems behaves as

$$g(r,L)=L^{-2X}[Y(r)+Y(nL-r)](A+BL^{y_c}+CL^{y_i}), \tag{24}$$

with the function

$$Y(r)=(e^{hr/2R}-e^{-hr/2R})^{-2X}\quad(h=1+aL^{y_c}). \tag{25}$$

Here, the radius is $R=L/\pi$ as mentioned before.

Equations (24) and (25) were fitted to the Monte Carlo data. The value of y_c is fixed at -0.413 as specified above. For the magnetic and the energylike correlations, the exponent X represents the bulk magnetic and thermal scaling dimensions X_h and X_t, respectively. We obtain $X_h=0.5178(12)$ and $X_t=1.423(19)$, in a good agreement with the existing results $X_h=0.5185(3)$ and $X_t=1.413(1)$ [9,19–21]. This confirms the assumption of conformal invariance [7]. Including another correction cL^{y_i} in the function h does not improve the residual χ^2 of the fit significantly.

B. Binder cumulant on a spherocylinder

The dimensionless quantity originally introduced by Binder plays an important role in the study of critical phenomena [22]. An example is Ref. [8], in which we obtain the length ratio $\alpha_0=0.881(6)$ by sampling the Binder cumulant. For a system on a hypercubic lattice in general d dimensions, the universal ratio Q, which is closely related to the Binder cumulant [22], is defined as

$$Q(K)=\langle\sigma^2\rangle^2/\langle\sigma^4\rangle. \tag{26}$$

For a system on a hypercylinderlike geometry $S^{d-1}\times\mathbb{R}^1$, however, another definition is desirable. The reason is as follows. If the length of the geometry $S^{d-1}\times\mathbb{R}^1$ is much larger than the correlation length, i.e., $\gamma=L/R\to\infty$, the critical magnetization density is normally distributed, and thus the value of $Q(K)$ approaches 1/3. The same value applies to a disordered system. As a consequence, little information can be obtained for critical phenomena. In this case, a useful dimensionless quantity can be defined as [4,23]

$$G(K,\gamma)=(3-\langle\sigma^4\rangle/\langle\sigma^2\rangle^2)\,\gamma/3, \tag{27}$$

which plays a similar role as the aforementioned correlation length ξ_R. According to finite-size scaling, the critical quantity G is universal for infinite systems R and $\gamma\to\infty$.

In two dimensions, the critical bulk two- and four-point correlation functions are exactly known for the Ising model [24]. On this basis, the value of G for the surface of an infinitely long cylinder can be calculated according to the prediction of conformal invariance. This calculation has been performed by Burkhardt and Derrida [23], who evaluated the resulting integrals by a Monte Carlo method. Their result is

$$G(K_c,\infty)/2\pi=2.46044(2). \tag{28}$$

For an arbitrary model, it was shown by Cardy [25] that for the infinitely long strip

$$G(K_c,\infty)/2\pi\sim(\pi X_h)^{-1}, \tag{29}$$

if X_h is small.

In three dimensions, no result for the quantity G is available yet. Here, we sampled both quantities Q/π and G/π on a spherocylinder as a function of the size L and the ratio $\gamma/\pi=n$. The system sizes were taken as $L=8,10,12,16,20,24,30,40$ and the largest value of n is 20. Periodic boundary conditions were applied in the u direction. Part of the results is shown in Figs. 1 and 2. The latter figure suggests that $n=8$ already provides a good approximation of the geometry $S^2\times\mathbb{R}^1$.

For finite systems at the critical point, we fitted the following formula to the Monte Carlo data:

$$G(L,n)/\pi=G_\infty+\frac{a_1}{n}+\frac{a_2}{n^2}+v(nL)^{y_c}+\cdots. \tag{30}$$

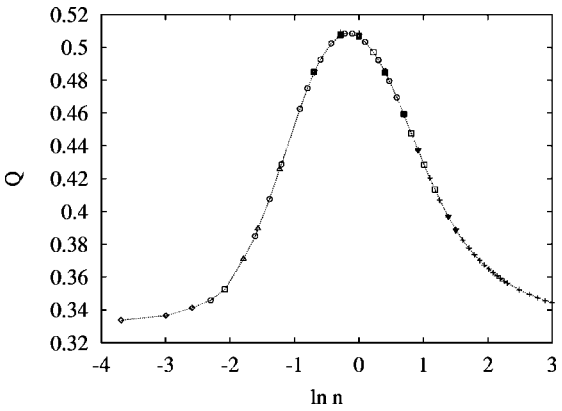

FIG. 1. The dimensionless ratio Q, shown as a function of $\ln n$, where $n\pi$ is the ratio of the length to the radius of the spherocylinder. Systems sizes are $L=8$ (+), $L=12$ (∇), $L=16$ ($\square$), $L=20$ ($\bigcirc$), $L=24$ ($\triangle$), and $L=40$ ($\diamond$). The data collapse indicates that corrections to scaling are small.

In order to obtain an acceptable residual χ^2 of the fit, we applied a cutoff by excluding small system sizes $L\leqslant 6$ and $n\leqslant 5$. The result is $G/\pi=0.6458(5)$, which differs significantly from that for a two-dimensional strip [23].

C. Spherocylinder with fixed boundary conditions

Fixed boundary conditions, i.e., infinitely strong fields, were imposed on both ends of the spherocylinder ($u=0$ and $u=nL$). The finite system sizes were taken as $L=4,6,8,10,12,14,16,20,24$ and $n=8$. The magnetization and the energy densities,

$$m(r)=\frac{1}{V}\sum_{\theta}\int_0^{2\pi}d\varphi\,\frac{L}{\pi}\sin\theta\langle\sigma(r,\theta,\varphi)\rangle \tag{31}$$

and

$$e(r)=\frac{1}{V}\sum_{\theta}\int_0^{2\pi}d\varphi\,\frac{L}{\pi}\sin\theta\langle n(r,\theta,\varphi)\rangle, \tag{32}$$

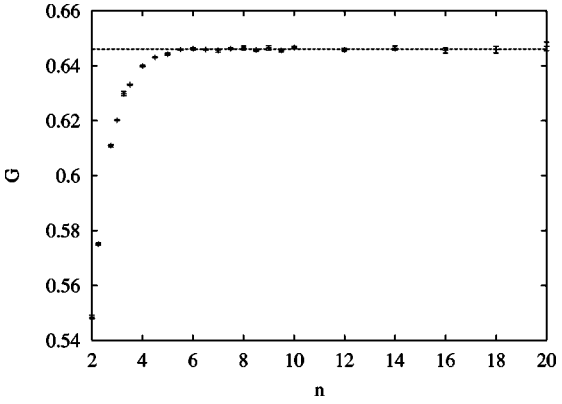

FIG. 2. The dimensionless ratio G, shown as a function of n, where $n\pi$ is the ratio of the length to the radius of the spherocylinder. System size is $L=8$.

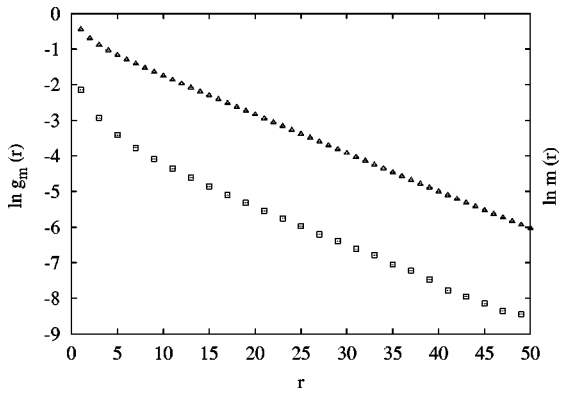

FIG. 3. The quantities $\ln m(r)$ ($\square$) and $\ln g_m(r)$ ($\triangle$), the logarithms of the magnetization profile and of the magnetic correlation, respectively, vs the distance r along a spherocylinder with $R=16/\pi$ and $n=8$. The errorbars for $\ln m(r)$ are smaller than the symbol size; for $\ln g_m(r)$, these are at most approximately equal to the symbol size.

were sampled. Here, we have chosen the density of the interfaces $n(r,\theta,\varphi)$ as the energy density. Compared to the alternative definition of e in Eq. (21), sampling the density of the interfaces consumes much less computer time. This is due to the fact that, during the Monte Carlo simulations, the positions of these interfaces are stored in computer memory as the dynamical variables.

The scaling behavior of $m(r)$ and $e(r)$ follows from Eq. (14). According to Eqs. (14) and (7), the magnetization density $m(r)$ and the correlation $g_m(r)$ decay in a similar way with respect to the distance r. An example is shown in Fig. 3. For a given spherocylinder with radius R, however, the prefactor of $g_m(r)$ is R^{-2X_h} [Eq. (7)] while that of $m(r)$ is R^{-X_h} [Eq. (14)]. This effect, combined with the fact that less computer time is needed, shows that $m(r)$ is a better quantity than $g_m(r)$ to determine the magnetic scaling dimension. A similar argument holds for the energy density. Taking into account finite-size corrections and fixed boundary conditions at both ends, we have

$$m(r,L)=L^{-X_h}[Y(r)+Y(nL-r)](A+BL^{y_c}) \tag{33}$$

and

$$e(r,L)=n_0+L^{-X_t}[Y(r)+Y(nL-r)](A+BL^{y_c}), \tag{34}$$

where n_0 is the bulk density of the interfaces at criticality and the function $Y(r)$ is given in Eq. (25).

Formulas (33), (34), and (25) were fitted to the Monte Carlo data. An example of the energy density is shown in Fig. 4. The value of n_0 is fixed at 0.901 60(5), as obtained from numerical simulations in a flat geometry. We obtain $X_h=0.5182(6)$ and $X_t=1.419(7)$. The precision of these results is comparable to that of other methods [9,19–21].

D. Half spherocylinder $S^1\times S^+\times R^1$

For the half spherocylinder, fixed and free boundary conditions were applied on both ends ($u=0$ and $u=nL$) and the equators ($\theta=\pi/2$) of $S^1\times S^+$, respectively. The systems

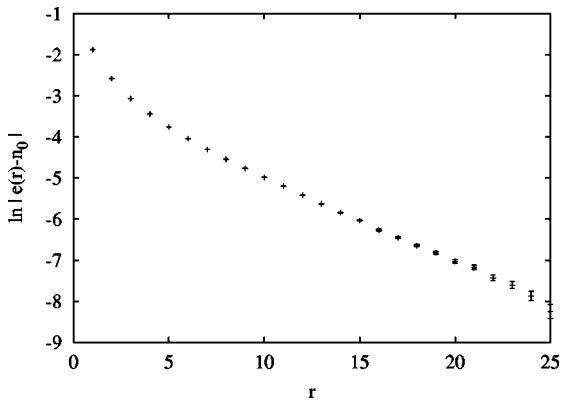

FIG. 4. Exponential decay of the interface density, shown as $\ln|e(r)-n_0|$ vs the distance r along a spherocylinder with $R=24/\pi$ and $n=8$. Errorbars show the statistical uncertainty.

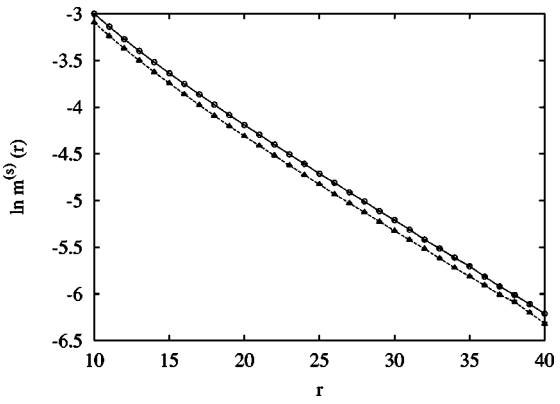

FIG. 5. Exponential decay of the surface magnetization density, shown as $\ln m^{(s)}(r)$, vs the distance r along a conventional solid cylinder ($\triangle$) and a spherocylinder ($\bigcirc$). The radii of these two objects are $R=19.5$ and $19.5\times 2/\pi$, respectively; the ratio is $n=8$.

sizes were taken as $L=8,10,12,\ldots,26$ and $n=8$. The radius of the half spherocylinder is $R=(2L-1)/\pi$, different from the formula $R=L/\pi$ for the spherocylinder. The magnetization density on the equators was sampled, defined as

$$m^{(s)}(r)=\frac{1}{2\pi}\int_0^{2\pi} d\varphi\langle\sigma(r,\pi/2,\varphi)\rangle. \tag{35}$$

The finite-size scaling behavior of this surface magnetization densities also follows from Eq. (33), except that the exponent X_h is replaced by the surface scaling dimension $X_h^{(s)}$. Equations (33) and (25) were fitted to the Monte Carlo data, and a short-distance cutoff was applied. The minimum system size included in the fit is $L=14$. The result is $X_h^{(s)}=1.263(5)$, of which the precision is good in comparison with the known value obtained by a different method, $X_h^{(s)}=1.259(15)$ [26].

E. Conventional solid cylinder

We have also performed simulations inside a conventional solid cylinder with fixed and free boundary conditions on both ends ($u=0$ and $u=nL$) and the surface, respectively. The system sizes are $L=8,10,12,16,18$ and $n=8$. The radius of the cylinder is given by $R=L-1/2$ in this case, which differs by a factor $\pi/2$ from that of the half spherocylinder with the same L. The surface magnetization density $m^{(s)}(r)$ along the cylinder was sampled. We found, empirically, that the decay of $m^{(s)}(r)$ along the conventional cylinder is very similar to that along the half spherocylinder $S^1\times S^+\times\mathbb{R}^1$ with the same finite size L. An example is shown in Fig. 5. Thus, we also fitted the Monte Carlo data on the basis of Eqs. (33) and (25), but with $h=\zeta+aL^{y_c}$. Here, the factor ζ accounts for the difference between the surface correlation length along the solid cylinder and that along the aforementioned half spherocylinder. The value of $X_h^{(s)}$ is fixed at 1.263 as specified earlier, and we obtain $\zeta=1.585(9)$, very close to $\pi/2\simeq 1.571$.

V. DISCUSSION

We have shown how one can simulate the Ising model in curved geometries by means of a continuous cluster Monte Carlo algorithm. We confirm that the three-dimensional Ising model is conformally invariant. The satisfactory precision of the numerical results presented in this paper shows that, as in two dimensions, conformal mappings also provide a useful tool to investigate critical phenomena (at least, if one takes the assumption of conformal invariance for granted). Further applications to other models, such as the bond percolation model, are also possible [27].

We have used the same algorithm for Monte Carlo simulations of a system inside a conventional solid cylinder. We found that the corresponding surface correlation length differs by a factor close to $\pi/2$ from that along a half spherocylinder. However, it is not obvious that this result can be supported by means of a conformal transformation.

ACKNOWLEDGMENTS

This research was supported by the Dutch FOM foundation (''Stichting voor Fundamenteel Onderzoek der Materie'') which is financially supported by the NWO (Nederlandse Organisatie voor Wetenschappelijk Onderzoek).

[1] A.A. Belavin, A.M. Polyakov, and A.B. Zamolodchikov, J. Stat. Phys. **34**, 763 (1984).
[2] D. Friedan, Z. Qiu, and S. Shenker, Phys. Rev. Lett. **52**, 1575 (1984).
[3] T.W. Burkhardt and I. Guim, Phys. Rev. B **47**, 14 306 (1993), and references therein.
[4] J.L. Cardy, in *Phase Transitions and Critical Phenomena*, edited by C. Domb and J.L. Lebowitz (Academic Press, London, 1987), Vol. 11, p. 55.
[5] J.L. Cardy, J. Phys. A **17**, L385 (1984).
[6] J.L. Cardy, J. Phys. A **18**, L757 (1985).
[7] Y. Deng and H.W.J. Blöte, Phys. Rev. Lett. **88**, 190602 (2002).

[8] H.W.J. Blöte and Y. Deng, Phys. Rev. E **66**, 066110 (2002).
[9] Y. Deng and H.W.J. Blöte, Phys. Rev. E **67**, 036107 (2003).
[10] M. Weigel and W. Janke, Europhys. Lett. **51**, 578 (2000).
[11] T.W. Burkhardt and E. Eisenriegler, J. Phys. A **18**, L83 (1985).
[12] H.F. Trotter, Proc. Am. Math. Soc. **10**, 545 (1959).
[13] M. Suzuki, Prog. Theor. Phys. **56**, 1454 (1976).
[14] P.W. Kasteleyn and C.M. Fortuin, J. Phys. Soc. Jpn. **26**, 11 (1969).
[15] R.H. Swendsen and J.-S. Wang, Phys. Rev. Lett. **58**, 86 (1987); J.-S. Wang and R.H. Swendsen, Physica A **167**, 565 (1990).
[16] U. Wolff, Phys. Rev. Lett. **62**, 361 (1989); Phys. Lett. B **228**, 379 (1989).
[17] W.H. Zheng, J. Oitmaa, and C.J. Hamer, J. Phys. A **27**, 5425 (1994).
[18] R. Rieger and N. Kawashima, Eur. Phys. J. B **9**, 233 (1999).
[19] H.W.J. Blöte, L.N. Shchur, and A.L. Talapov, Int. J. Mod. Phys. C **10**, 1137 (1999).
[20] P. Butera and M. Comi, Phys. Rev. B **56**, 8212 (1997).
[21] R. Guida and J. Zinn-Justin, J. Phys. A **31**, 8103 (1998).
[22] K. Binder, Z. Phys. B: Condens. Matter **43**, 119 (1981).
[23] T.W. Burkhardt and B. Derrida, Phys. Rev. B **32**, 7273 (1985).
[24] L. Onsager, Phys. Rev. **65**, 117 (1944).
[25] J.L. Cardy, Nucl. Phys. B **270**, 186 (1986).
[26] M.P. Nightingale and H.W.J. Blöte, Phys. Rev. B **48**, 13 678 (1993).
[27] Y. Deng and H.W.J. Blöte (unpublished).